Mathematical Biology

From *Staphylococcus aureus* gene regulation to its pattern formation

A. Oelker[1] · T. Horger[1] · C. Kuttler[1]

Abstract

The focus of this paper is to develop a new partial differential equation model for the pattern formation of the human pathogen *Staphylococcus aureus*, starting from a newly developed model of selected gene regulation mechanisms. In our model, we do not only account for the bacteria densities and nutrient concentrations, but also for the quorum sensing and biofilm components, since they enable bacteria to coordinate their behavior and provide the environment in which the colony grows. To this end, we model the relevant gene regulation systems using ordinary differential equations and therefrom derive our evolution equations for quorum sensing and biofilm environment by time-scale arguments. Furthermore, we compare and validate our model and the corresponding simulation results with biological real data observations of *Staphylococcus aureus* mutant colony growth in the laboratory. We show that we are able to adequately display the qualitative biological features of pattern formation in selected mutants, using the parameter changes indicated by the gene regulation mechanisms.

Keywords Pattern formation · Mathematical modeling · *Staphylococcus aureus* · Quorum sensing · Biofilm · Finite element simulation

Mathematics Subject Classification 92B05 · 93A30 · 92C15 · 35Q80 · 68U20

1 Introduction

The bacterium *Staphylococcus aureus* (*S. aureus*) is a Gram-positive, non-sporulating bacterium found in nature and on mammal skin. Its pathogenic form is of specific

✉ A. Oelker
  oelker@ma.tum.de

  T. Horger
  horger@ma.tum.de

  C. Kuttler
  kuttler@ma.tum.de

1   Technische Universität München, Boltzmannstrasse 3, 85748 Garching bei München, Germany

interest due to its role in hospital-acquired infections from medical devices like pros-
thetics or surgical instruments (Bronner et al. 2004). In these infections the formation
of biofilm is crucial to bacterial survival. Pattern formation in Gram-positive bacteria
has been studied regarding biology and mathematical modeling, e.g. by Ben-Jacob
et al. (2001), García-Betancur et al. (2017), Matsushita et al. (1999) and Mimura et al.
(2000), often for the close *S. aureus* relative *B. subtilis*, e.g. by Dervaux et al. (2014),
Kawasaki et al. (1997), Seminara et al. (2012) and Vlamakis et al. (2013). In this
paper, we develop a new partial differential equation (PDE) model for the pattern for-
mation in *S. aureus*, including nutrient concentration, replicative and non-replicative
bacteria densities, quorum sensing substance and biofilm environment concentration.
Therefore, we consider gene regulation mechanisms leading to the production of the
representative substances autoinducing peptide (AIP) and polysaccharide intercellu-
lar adhesin (PIA) involved in *S. aureus* quorum sensing and biofilm formation. The
complex regulation systems are described by ordinary differential equations (ODE)
and the resulting model is subsequently reduced with the aim of using the derived
equations in the description of bacterial pattern formation.

   In this context, biofilm formation is crucial since in our modeling the biofilm
constitutes the environment in which the bacterial colony grows and develops its
characteristic features. We note that in our modeling the term biofilm does not denote
the entire biomass as in the classical sense, it is only the environment in which the
bacteria live and it is considered as a product of the replicative bacteria which does
not grow on its own. In addition, quorum sensing (QS) is a cell–cell communication
mechanism, which coordinates gene expression and behavior in bacterial populations,
depending on population densities (Fuqua et al. 1994; Müller et al. 2006; Perez-
Velazquez et al. 2016). In *S. aureus*, the QS signalling molecule AIP is produced by
the *agr* operon (Boles and Horswill 2008; Yarwood and Schlievert 2003; Yarwood
et al. 2004). AIP impedes the attachment and development of a biofilm (Boles and
Horswill 2008). An increasing concentration of NaCl in the experimental set up leads
to increased biofilm formation and lower growth rates and the availability of nutrients
is thus linked to commitment towards biofilm dispersal (Mhatre et al. 2014). During
population growth, on top of the biofilm a thin film of liquid is formed.

   From a mathematical perspective, general quorum sensing and gene regulation at
the *agr* operon are studied by Ward et al. (2001) and by Jabbari et al. (2010, 2012a, b),
respectively. In the paper by Jabbari et al. (2010), an ODE model of the *agr* operon is
established and equation systems are asymptotically analyzed on different time scales.
A goal in the following is to derive PDE for the QS substance AIP and the biofilm
substance PIA and terms for the diffusion coefficients for the nutrients and replicative
bacteria. The modeling of the nutrient concentration and bacteria densities is based on
the approach for pattern formation in *S. aureus* by García-Betancur et al. (2017). The
rest of the paper is structured as follows: In Sect. 2, we introduce our ODE system for
the gene regulation mechanisms in *S. aureus* and perform the model reduction, which
yields the reaction terms for the quorum sensing substance and biofilm equations in
the pattern formation PDE model. In Sect. 3, we verify that our model adequately
predicts colony shapes for *S. aureus* mutant colonies by comparing our simulation
results to biological observations of colony growth in the laboratory.

2 Mathematical modeling

In the paper by García-Betancur et al. (2017) a system of four equations was introduced, which takes into account nutrient concentration, replicative and non-replicative bacteria densities and quorum sensing substance concentration. Bacteria in the reproductive state are assumed to move according to a mixed diffusion dispersal term, while bacteria in the non-replicative state only change locations through pushing induced by the movement of the replicative bacteria. However, the model by García-Betancur et al. (2017) includes a generic quorum sensing term and does not take into account biofilm formation and the related effects, which are crucial to colony growth.

Our newly developed model is based on the structure as introduced in García-Betancur et al. (2017), but with two major changes: there is a separate variable and equation included for the biofilm component, separate from the two bacterial components. Secondly, the details of the biologically known underlying gene regulation mechanisms are taken into account. With this improved understanding we aim for additional predictions, which associate parameter changes for a certain mutant to gene regulation effects. Thus, in the following we choose the terms unrelated to QS and biofilm formation as introduced by García-Betancur et al. (2017) and aim to determine formulations for $f_2(b, q)$, $f_3(n, b, q, f)$, $D_1(f)$ and $D_2(n, b, q)$ in our system of the form

$$\frac{\partial n}{\partial t} = \nabla \cdot (D_1(f)\nabla n) - G_1 \frac{nb}{1+\gamma n}\left(1 + \frac{1}{q_m + \delta q}\right), \tag{1}$$

$$\frac{\partial b}{\partial t} = \nabla \cdot (D_2(n, b, q)\nabla b) + G_2 \frac{nb}{1+\gamma n}\left(1 + \frac{1}{q_m + \delta q}\right) - \varepsilon \frac{b}{(1+\frac{b}{a_1})(1+\frac{n}{a_2})}, \tag{2}$$

$$\frac{\partial s}{\partial t} = \nabla \cdot \left(\tau \frac{b}{b+b_s}\nabla s\right) + \varepsilon \frac{b}{(1+\frac{b}{a_1})(1+\frac{n}{a_2})}, \tag{3}$$

$$\frac{\partial q}{\partial t} = d_q \Delta q + f_2(b, q), \tag{4}$$

$$\frac{\partial f}{\partial t} = d_f \Delta f + f_3(n, b, q, f), \tag{5}$$

where n, b, s, q and f denote the nutrient concentration, the replicative and non-replicative bacteria densities, the AIP concentration and the biofilm environment concentration, which in our case corresponds to the concentration of PIA used as an indicator for biofilm. Note that we assume the diffusion of non-replicative bacteria to be driven by the movement of the replicative cells, which push the non-replicative bacteria in a limited process. In the case $b \gg b_s$, the diffusion of the non-replicative bacteria becomes approximately linear. However, there is only a fixed amount of nutrients in the system and if $b \gg b_s$, these nutrients are consumed very fast. This results in a fast conversion of replicative bacteria to non-replicative bacteria, such that the threshold b_s holds again. For a detailed discussion of the remaining diffusion coefficients we refer to Sect. 2.6. Furthermore, nutrient availability influences

Table 1 Parameters for the regulation of an example substance from gene locus $\star$

Parameter	Rate constant for	Parameter	Rate constant for
$b_\star$	Gene locus up-regulation	$u_\star$	Gene locus down-regulation
$m_\star$	Basal production of mRNA	$v_\star$	Regulation-induced transcription
$\delta_\star$	Degradation and dilution	$\kappa_\star$	Translation

colony structure in that nutrient gradients drive colony growth and in that the availability of nutrients determines the transition of bacteria from the replicative to the non-replicative state. Additionally, it should be noted here that the spatial processes have been non-dimensionalized following the procedure introduced in Kawasaki et al. (1997).

QS systems regulate the behavior of the bacterial population in response to the density. *S. aureus* performs QS via the *agr* operon, which is only found in the *Staphylococcus* genus (Gray et al. 2013), and the *luxS* system, which is common for many bacterial species (Xu et al. 2006). The *agr* system uses the signaling substance AIP. It represses biofilm formation and influences the structure of a biofilm through the regulation factors PSM-α, PSM-β and δ-toxin. The *luxS* system in *S. aureus* uses the signalling substance AI-2 and regulates the gene transcription of CP5, a capsular polysaccharide (CP) cell wall component responsible for interaction with the host immune system during the invasive process (Zhao et al. 2010). Since we consider bacterial growth in a laboratory setting, this pathway is not included into the model. Following the paper by Jabbari et al. (2010), we assume that the system is developed for the situation of a well-mixed environment with sufficient supply of ribosomes, such that at each pass the entire strand of mRNA is translated.

We assume that a proportion of the cells is up-regulated for the activity of a regulatory system, such as *agr*. The gene up-regulation at a locus is increased by the binding of external substances to the promoters. Down-regulation is proportional to the number of up-regulated cells and the gene locus down-regulation rate is increased by the binding of further substances. An overview of the recurring parameters for an example gene locus is found in Table 1. Furthermore, in Fig. 1 an overview of the gene regulation circuits in *S. aureus* is depicted, showing regulation mechanisms in the *agr*, the *ica*, the *sarA* and the *sarA* homologue regulation systems (Audretsch et al. 2013; Bronner et al. 2004; Jabbari et al. 2010; Periasamy et al. 2012).

2.1 The *agr* system

The *agr* system, depicted in the red area in Fig. 1, is considered in detail as an example of a subsystem of gene regulation. It is responsible for the production of the QS substance AIP. In Fig. 1 we observe that the activity of the *agr* operon is positively influenced by the concentrations of mRNAIII (R_3), SarA ([$SarA$]), SarU ([$SarU$]) and phosphorylated AgrA (A_P) and negatively influenced by the concentration of σ^B (Bischoff et al. 2001). We model this by introducing the factors $[agr+] := R_3 + [SarA] + [SarU] + A_P$ and $[agr-] := [\sigma^B]$ in an equation of the form
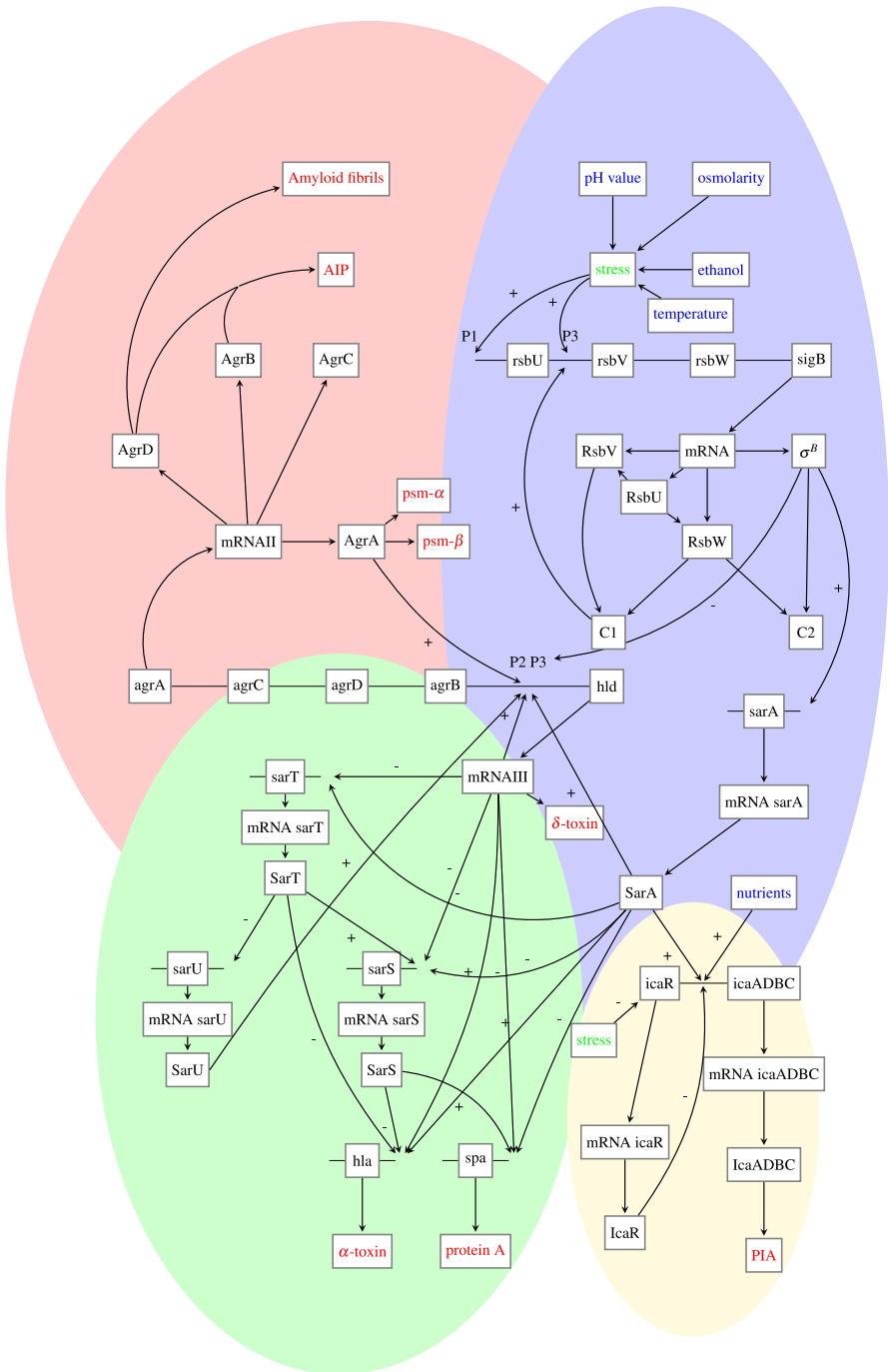
Fig. 1 Gene regulation in *S. aureus*. External influences written in blue, resulting variable stress written in green and output substances of a cell colony in red. The red, blue, green and yellow areas indicate the *agr*, *sarA*, *sarA* homologue and *ica* regulation subsystems, respectively (colour figure online)
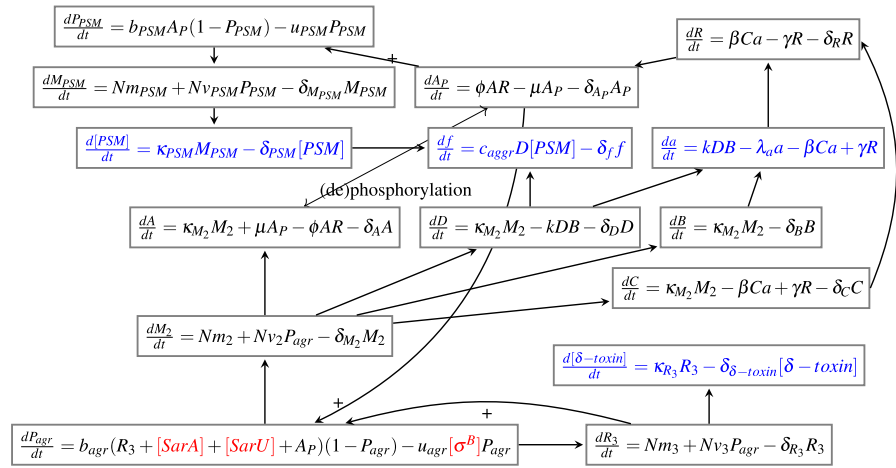
Fig. 2 Gene regulation in the *S. aureus agr* subsystem. System influences in red, equations for output variables in blue (colour figure online)

$$\frac{dP_{agr}}{dt} = b_{agr}[agr+](1 - P_{agr}) - u_{agr}[agr-]P_{agr}$$

for the proportion $P_{agr} \in [0, 1]$ of cells with up-regulated *agr* activity. We note that if the proportion of up-regulated cells is zero, then $\frac{dP_{agr}}{dt} > 0$ and no further down-regulation takes place. In the same way at $P_{agr} = 1$ no further up-regulation is possible. This equation is of special interest since it represents the regulation of the activity of the *agr* subsystem, which is involved in the production of AIP. Within the *agr* subsystem further interactions take place, which are represented in the system of equations displayed in Fig. 2.

Our model of the *agr* operon depicted in Fig. 2 is based on the model developed by Jabbari et al. (2010), as we consider similar interactions but fewer equations. In the equation for mRNAII (M_2) in Fig. 2 we model that each of the N bacteria in the system produces M_2 at the basal production rate m_2. Increased activity of the *agr* operon up-regulates this production at the velocity v_2. Degradation and dilution take place at the rate δ_{M_2}. Furthermore, we see that the proteins AgrB (B), AgrD (D), AgrC (C) and AgrA (A) are produced by translation of mRNAII. While AgrB is a membrane protein, AgrA can be phosphorylated by AgrC with bound AIP and the QS substance AIP is produced from AgrD under the influence of AgrB. Since the entire strand of mRNA is translated at each pass, we take the translation rates to be of the same order. As in the paper by Jabbari et al. (2010), the variables a, A_P and R denote the amounts of AIP, phosphorylated AgrA and AIP-bound AgrC, respectively. The binding of AIP to AgrC is modeled as $\pm \beta Ca$ and this binding is assumed to be reversible ($\pm \gamma R$). The phosphorylation and dephosphorylation of AgrA are modeled as ϕAR and μA_P. Degradation of AIP takes place outside the cells with the corresponding degradation rate λ_a. The P3 operon is responsible for the formation of the untranslated RNAIII, an intracellular effector, which up-regulates extracellular protein genes and down-regulates cell wall colonisation factor genes (Jabbari et al. 2010). RNAIII experiences

transcription but not translation, and can thus base pair with other mRNA strains in order to inhibit encoding of virulence factors (Waters and Storz 2009).

In a similar way, we model the production of the biofilm-promoting hydrophobic phenol soluble modulins (PSM), which are responsible for biofilm structuring (Schwartz et al. 2012) and dispersal and the production of amyloid fibrils (Schwartz et al. 2014). Due to their amphipathic α-helical structure, PSM can lyse eukaryotic cells, such as neutrophils, monocytes, and erythrocytes, by non-specific destruction of biological membranes (Duong et al. 2012). The regulation of P_{PSM} takes place by direct binding of the AgrA response regulator (Peschel and Otto 2013; Queck et al. 2008). For P_{PSM}, we obtain the equation

$$\frac{dP_{PSM}}{dt} = b_{PSM} A_P (1 - P_{PSM}) - u_{PSM} P_{PSM}.$$

While the proportions of up-regulated cells are dimensionless quantities, the dimensional model includes concentrations of molecules per volume unit (cm^3 or mm^3) for all proteins and RNAs and the rates are measured per second. We adjust for the additional units by choosing appropriate units for the corresponding rate constants, e.g. the constant k in the production of AIP from AgrD and AgrB has the unit $[k] = \frac{\text{cm}^3}{\text{molecules} \cdot \text{second}}$.

We non-dimensionalize the model for the simulations in order to reduce the number of parameters, using the timescale $\tau := \delta_{M_2} t$ for all subsystems, where we assume that the degradation rates of the considered mRNAs are of similar order, i.e. $\delta_{M_2} = \delta_{R_3} = \delta_{M_{PSM}} = \delta_{M_{RsbU}} = \delta_{M_{ica1}} = \delta_{M_{sarT}}$. As an example of the non-dimensionalization we consider the *agr* subsystem. As in the paper by Jabbari et al. (2010), the non-dimensionalization is performed with respect to the starting values calculated as the stationary points for $k = 0$ and $P_{agr} = P_{PSM} = 0$. Due to $k = 0$, we obtain $a(0) = R(0) = A_P(0) = 0$, which allows to choose the non-dimensionalizations for these variables as $a' := \frac{\delta_{M_2} \delta_D}{Nm_2 \kappa_{M_2}} a$, $A'_P := \frac{\delta_{M_2} \delta_A}{Nm_2 \kappa_{M_2}} A_P$ and $R' := \frac{\delta_{M_2} \delta_C}{Nm_2 \kappa_{M_2}} R$. Also following Jabbari et al. (2010), we assume that dilution dominates degradation and thus the δ_X are of the same order for all proteins X. We obtain the new parameters $\lambda := \frac{\delta_X}{\delta_{M_2}}$ and $\eta := \frac{\delta_D}{\delta_C} \approx 1$. We furthermore reconsider the activation and deactivation factors as well since, due to the new timescale, the variables are rescaled. Thus we define

$$[agr+]' := \beta_{agr}(R'_3 + \alpha([SarA]' + [SarU]' + A'_P)) \tag{6}$$

with $\beta_{agr} := \frac{Nm_3}{\delta_{R_3}}$, which yields $b'_{agr} := b_{agr} \beta_{agr}$ and $\alpha := \frac{\kappa_X}{\delta_X}$, assumed to be equal for $X \in \{[SarA], [SarU], A_P\}$. The obtained non-dimensional equations are depicted in Fig. 3 and, for ease of notation, we omit the primes and directly state the equations for the remaining subsystems in their non-dimensional forms.
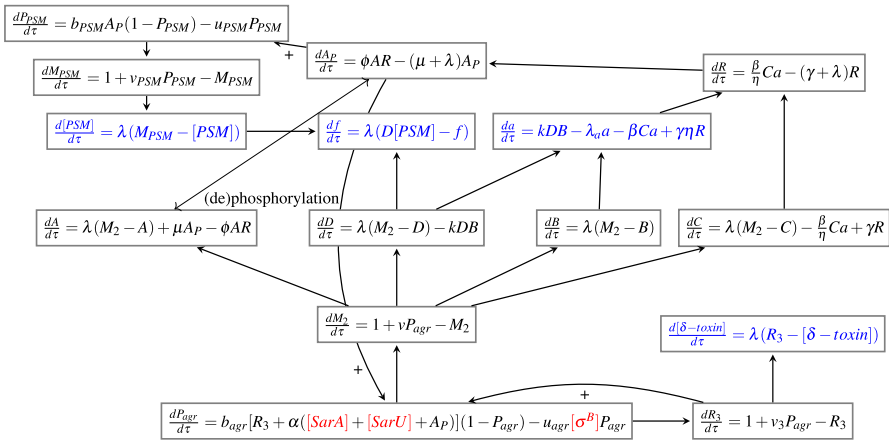
Fig. 3 Nondimensional differential equations for gene regulation in the *S. aureus agr* subsystem. System influences in red, equations for output variables in blue (colour figure online)

2.2 The *sarA* system

We see in Fig. 1 that regulation of the *sarA* system in the blue area depends on the environmental conditions of the colony, including the temperature T, the osmolarity and the pH level of the environment (Vuong et al. 2005). We summarize these factors as the stress on the system, denoted by $[str] \in [0, 1]$, and include it into our model system as one single variable

$$[str] := \alpha |T - T_{\text{ref}}| + \beta[\text{osmolarity}] + \gamma |\text{pH} - \text{pH}_{\text{ref}}| + \delta[\text{ethanol}],$$

with the optimal reference temperature T_{ref} and pH-value pH_{ref}. In Fig. 1, we observe that the parameter $[str]$ influences transcription of *rsbU*, *rsbV*, *rsbW* and *sigB*. As described above, the staphylococcal accessory regulator SarA activates transcription at the *agr* operon. In addition, also *S. aureus* biofilm formation depends on SarA and σ^B (Valle et al. 2003).

We see in Fig. 1 that transcription at the *sarA* operon is positively regulated by σ^B (Cheung and Manna 2005). Furthermore, SarA activates its own expression (Bronner et al. 2004), but this is neglected here for the sake of model simplification. We introduce proportions of up-regulated cells P_{RsbU} for the RsbU- and P_σ for the RsbV-, RsbW- and σ^B-production as well as the proportion P_{sarA} for the production of SarA. The resulting equations on the timescale τ are

$$\frac{dP_{RsbU}}{d\tau} = b_0[str](1 - P_{RsbU}) - u_0 P_{RsbU}, \tag{7}$$

$$\frac{dP_\sigma}{d\tau} = (b_0 + b_\sigma[C_1])[str](1 - P_\sigma) - u_0 P_\sigma, \tag{8}$$

$$\frac{dP_{sarA}}{d\tau} = b_{sarA}[\sigma^B](1 - P_{sarA}) - u_{sarA} P_{sarA}, \tag{9}$$
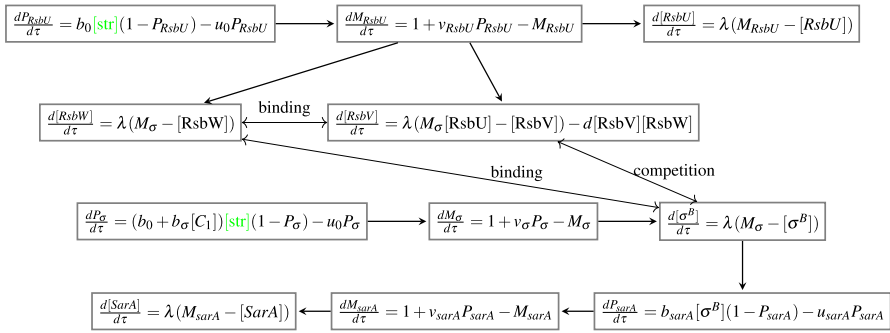
Fig. 4 Differential equations derived from gene regulation in the *S. aureus sarA* subsystem with σ^B. External influences in green (colour figure online)

where the origin of the factor $[C_1]$ is considered in detail in the following. An overview of the non-dimensional equations describing the interactions within the *sarA* subsystem is displayed in Fig. 4, where the equations are developed analogously to Sect. 2.1.

Basal transcription of the genes *rsbU*, *rsbV*, *rsbW* and *sigB* takes place at the σ^A-dependent promoter $sigB_{P1}$, and the genes *rsbV*, *rsbW* and *sigB* are also transcribed from the σ^B-dependent promoter $sigB_{P3}$ (Senn et al. 2005). Both promoters show a rapid response to environmental stress (Senn et al. 2005). Therefore we distinguish between the variables P_{RsbU} and P_σ in (7)–(8). The *rsbU* gene product, in combination with the *rsbV* and *rsbW* gene products, influences the expression of the σ^B-operon, responsible for the regulation of *sarA* transcription, in a competitively inhibitory process. In the regulation of *rsbU* activity in *S. aureus*, the RNA polymerase (RNAP) core enzyme and the σ^B-factor can associate to form an RNAP holoenzyme (Senn et al. 2005), which recognizes promoter regions in the DNA, initiating transcription at the $sigB_{P3}$ promoter (Dervaux et al. 2014). If the environmental stress on the system is low, RsbW binds to σ^B at rate k_2, keeping it from aggregating to the RNAP core enzyme and forming the complex C_2. If the stress increases, RsbU dephosphorylates RsbV, such that RsbV can bind to RsbW in order to release activated σ^B-factor, which then binds to the RNAP core enzyme and forms an RNAP holoenzyme (Knobloch et al. 2004). Thus σ^B and RsbV compete for the binding with RsbW. The RsbV–RsbW complex C_1 forms at rate k_1. All bindings occurring at rate k_i, $i \in \{1, 2\}$ are reversible at rate k_{-i}. In this framework we formulate the dimensional equations

$$\frac{d[C_1]}{dt} = -k_{-1}[C_1] + k_1[RsbW][RsbV], \quad \frac{d[C_2]}{dt} = -k_{-2}[C_2] + k_2[RsbW][\sigma^B].$$

(10)

With the stress-dependent rates $k_1 := [str]k_{-1}$ and $k_2 := (1 - [str])k_{-2}$, the binding and unbinding are assumed to be in equilibrium. Using $K_i := \frac{k_{-i}}{k_i}$, $i = 1, 2$, we obtain

$$K_1 = \frac{[RsbW][RsbV]}{[C_1]}, \qquad K_2 = \frac{[RsbW][\sigma^B]}{[C_2]}.$$

Due to mass conservation for σ^B, $[RsbV]$ and $[RsbW]$, it holds that

$$[\sigma^B] + [C_2] = \sigma_0, \qquad [RsbV] + [C_1] = v_0, \qquad [RsbW] + [C_1] + [C_2] = r_0,$$

where $\sigma_0, v_0, r_0 \in \mathbb{R}_+$ are constant parameters. Furthermore, as both $rsbV$ and $sigB$ are transcribed from the P3-operon, we approximate using $[RsbV] \approx [\sigma^B]$. We obtain

$$[C_1] = r_0 \frac{[RsbV][str]}{1 + [RsbV][str] + [\sigma^B](1 - [str])}$$
$$\approx r_0 \frac{[str]}{1/[RsbV] + [str] + (1 - [str])} \approx r_0[str].$$

Here we concentrate on the dependence on the system stress and take $r_0 = 1$ to insert $[C_1] \approx [str]$ in (8).

We see in Fig. 4 that we assume the amount of dephosphorylated RsbV to be a direct consequence of the availability of RsbU. Furthermore, we denote the binding of RsbW to RsbV with a constant rate as $-d[RsbW][RsbV]$. In the unstressed as well as in the stressed cell, the ratio of RsbV to phosphorylated RsbV (RsbV-P) is approximately 0.22 if RsbU is present. This ratio does not change significantly due to stress (Pane-Farre et al. 2009), and thus we do not model RsbV-P explicitly. Furthermore, the equations for RsbV, RsbW and σ^B are simplified considerably by taking into account that the equations in (10) are assumed to be in equilibrium.

2.3 The *ica* system

The *ica* locus is a part of the accessory genes found in most *S. aureus* strains (Cue et al. 2012; Arciola et al. 2015) and consists of the *icaR* and the *icaADBC* locus, which are transcribed divergently (Cue et al. 2012). It is of special interest since it is involved in the synthesis of the main extracellular polymeric substance (EPS) component polysaccharide intercellular adhesin (PIA). PIA controls intercellular adhesion during the initial stages of biofilm formation (Cue et al. 2012). Its synthesis is achieved by the combination of all products of the *icaADBC* gene cluster and modeled as depicted in Fig. 5. While IcaA and IcaD are necessary for the expolysaccharide synthesis, IcaC translocates the polymer poly-N-acetylglucosamine to the bacterial surface and IcaB deacetylates the molecule, enabling fixation to the bacterial cell surface (Cue et al. 2012). The *icaADBC* cluster genes are therefore modeled together.

Transcription at the *ica* operon is a direct consequence of the level of $SarA$, which binds to the *icaADBC* promoter region. The influence of σ^B is indirect (Cue et al. 2012) since the *ica* locus does not have a corresponding binding site (Cerca et al. 2008), and thus not considered here. Furthermore, an increasing nutrient concentration inhibits repression of *icaADBC* by IcaR (Cue et al. 2012). Since the nutrients do not bind to the promoter, we assume logistic up-regulation by nutrients. The IcaR dimers produced at the *icaR* locus bind in cooperative pairs to the *icaADBC* locus, where they inhibit transcription (Cue et al. 2012). For the transcription at the *icaR* locus, we assume
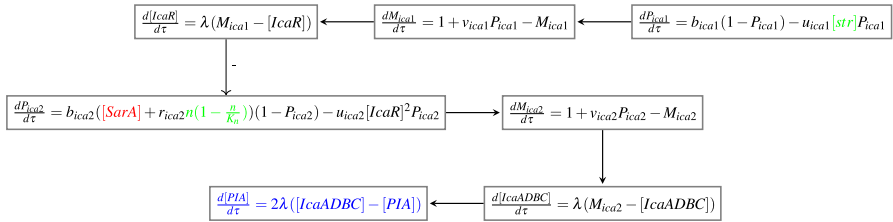
Fig. 5 Gene regulation in the *S. aureus ica* subsystem. External influences in green, system influences in red, equation for output variable in blue (colour figure online)

that, as in the close *S. aureus* relative *Staphylococcus epidermidis*, it is influenced by environmental stress. This is taken into account in the system of equations

$$\frac{dP_{ica1}}{d\tau} = b_{ica1}(1 - P_{ica1}) - u_{ica1}[str]P_{ica1},$$
$$\frac{dP_{ica2}}{d\tau} = b_{ica2}[ica2+](1 - P_{ica2}) - u_{ica2}[ica2-]P_{ica2},$$

where we introduce the regulation terms

$$[ica2+] := [SarA] + r_{ica2}n(1 - \frac{n}{K_n}) \quad \text{and} \quad [ica2-] := [IcaR]^2.$$

The regulations within the *ica* system in non-dimensional form are depicted in Fig. 5. Experimental evidence suggests that an intermediate substance exists, whose production is up-regulated by σ^B and down-regulated by SarA, and which either degrades PIA or represses PIA synthesis (Valle et al. 2003). We take the additional degradation term $\delta_{add}\frac{[\sigma^B]}{[SarA]}$ for PIA in the dimensional equation setting, which is close to δ_{add} if σ^B and SarA are present at similar levels, greater than δ_{add} if there is a higher level of σ^B and less than δ_{add} if there is more SarA. The amount of SarA is up-regulated by the amount of σ^B, and thus the fraction approaches δ_{add} as time increases, resulting in the additional degradation term δ_{add} in the equation for PIA.

2.4 The *sarA* homologue system

There are at least nine major SarA homologues, including SarR, SarS, Rot, SarT, SarU, SarV, MgrA, SarX and SarZ, where the gene loci *sarS* and *sarT* are adjacent, but transcribed divergently (Manna and Cheung 2003). The *sarA*, *sarT* and *sarU* genes are expressed evenly among strains (Ballal and Manna 2009) and thus included into our model. Furthermore the genes *mgrA*, *rot*, *sarZ*, *sarR* and *sarS* are expressed differently among strains (Ballal and Manna 2009) and thus only included through the *sarS* gene as their representative.

The production of protein A and α-toxin through the *sarA/agr* network (Schmidt et al. 2003) is steered by delicate interactions between the SarA homologues. SarA directly regulates the expression of *sarS* and *spa* as well as *sarT*. The transcription of
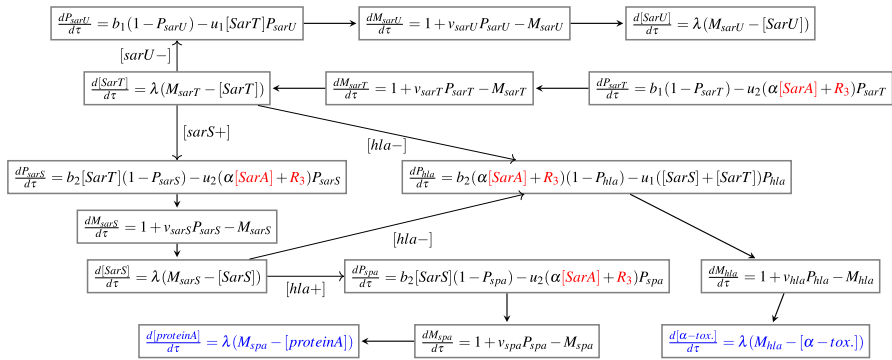
Fig. 6 Gene regulation in the *S. aureus sarA* homologue subsystem. System influences in red, equations for output variables in blue (colour figure online)

sarT is further reduced by a high activity of the *agr* system. SarT binds to the *sarS* promoter, increasing its activity and SarS influences the transcription of *spa*. Furthermore, the transcription of *hla* depends on the level of SarT. SarA binds to the Sar boxes within the promoter regions of the genes encoding protein A and α-toxin (Dunman et al. 2001) in the same way it binds to the promoter region for *agr*. In addition, mRNAIII regulates the transcription as well as the translation of α-toxin (Bronner et al. 2004). This yields the system of equations

$$\frac{dP_{sarT}}{d\tau} = b_1(1 - P_{sarT}) - u_2(\alpha[SarA] + R_3)P_{sarT},$$

$$\frac{dP_{sarU}}{d\tau} = b_1(1 - P_{sarU}) - u_1[SarT]P_{sarU},$$

$$\frac{dP_{sarS}}{d\tau} = b_2[SarT](1 - P_{sarS}) - u_2(\alpha[SarA] + R_3)P_{sarS},$$

$$\frac{dP_{spa}}{d\tau} = b_2[SarS](1 - P_{spa}) - u_2(\alpha[SarA] + R_3)P_{spa},$$

$$\frac{dP_{hla}}{d\tau} = b_2(\alpha[SarA] + R_3)(1 - P_{hla}) - u_1([SarS] + [SarT])P_{hla}.$$

An overview of the processes and resulting non-dimensional equations in the *sarA* homologue system is depicted in Fig. 6.

2.5 Model reduction

In this section, we perform the model order reduction, which is aimed at the derivation of ODE for the concentrations of free AIP (a) and PIA ($[PIA]$). The model reduction includes two main steps: the choice of the timescale of interest, which is the time scale of the change in the proportions of up-regulated cells P_{act}, where act $\in \{agr, PSM, RsbU, \sigma, sarA, ica1, ica2, sarT, sarU, sarS, spa, hla\}$, and the derivation of further simplifying parameter size considerations. A recurring structure in the regulation processes is the set of equations for P_{act}, M_{act} and a substance X.

The *agr* system constitutes a special case, since here mRNAII (M_2) and RNAIII (R_3) have to be considered. For details we refer to Fig. 3. Since the changes in M_{act} and X take place much faster than the changes in P_{act}, we introduce a parameter $\hat{\varepsilon} \ll 1$. Then the parameters b_{act} and u_{act} are in fact of the form $b_{\text{act}} = \hat{\varepsilon}\hat{b}_{\text{act}}$ and $u_{\text{act}} = \hat{\varepsilon}\hat{u}_{\text{act}}$, where $\hat{b}_{\text{act}}$ and $\hat{u}_{\text{act}}$ are $O(1)$, and we define the time scale of interest as $\hat{\tau} := \hat{\varepsilon}\tau$ to obtain

$$\frac{dP_{\text{act}}}{d\hat{\tau}} = \hat{b}_{\text{act}}[\text{act}+](1 - P_{\text{act}}) - \hat{u}_{\text{act}}[\text{act}-]P_{\text{act}}, \tag{11}$$

$$\hat{\varepsilon}\frac{dM_{\text{act}}}{d\hat{\tau}} = 1 + v_{\text{act}}P_{\text{act}} - M_{\text{act}}, \qquad \hat{\varepsilon}\frac{dX}{d\hat{\tau}} = \lambda(M_{\text{act}} - X). \tag{12}$$

In the limit $\hat{\varepsilon} \to 0$ we obtain a reduction of the system by two equations since $X = M_{\text{act}} = 1 + v_{\text{act}}P_{\text{act}}$, where $v_{\text{act}} = \text{const.}$. Then the evolution of X on the slow time scale is a direct consequence of the evolution of P_{act} since

$$\frac{dX}{d\hat{\tau}} = v_{\text{act}}\frac{dP_{\text{act}}}{d\hat{\tau}} = v_{\text{act}}\left(\hat{b}_{\text{act}}[\text{act}+](1 - P_{\text{act}}) - \hat{u}_{\text{act}}[\text{act}-]P_{\text{act}}\right).$$

We neglect differences among the speeds of those interactions that are faster than $\frac{dP_{\text{act}}}{d\hat{\tau}}$ since on the slow timescale, for both $\hat{\varepsilon} \to 0$ and $\hat{\varepsilon}^2 \to 0$ asymptotics, we approach the steady state. Only those concentrations which provide the connections between the different subsystems are required in an explicit form.

Furthermore for effective QS, the induced regulation has to take place faster than the regular effects. Thus there are also significant differences among the remaining rate constants. In agreement with Jabbari et al. (2010), we use $\varepsilon := \frac{m}{v} < 1$, the relationship between the basal mRNA transcription rate and the regulation-induced transcription for all subsystems. A possible value is $\varepsilon = 10^{-1}$. We obtain

$$v = \frac{\tilde{v}}{\varepsilon}, \quad \beta = \frac{\tilde{\beta}}{\varepsilon}, \quad \phi = \frac{\tilde{\phi}}{\varepsilon}, \quad \mu = \varepsilon\tilde{\mu}, \quad \lambda_a = \varepsilon\tilde{\lambda}_a, \tag{13}$$

for the *agr* system, where the parameters $\tilde{v}, \tilde{\beta}, \tilde{\phi}, \tilde{\mu}, \tilde{\lambda}_a$ are $O(1)$.

The connecting concentrations to the *agr* subsystem are the concentrations a and A_P of free AIP and phosphorylated AgrA. We apply the time-scale argument to the set of equations depicted in Fig. 3, calculate the concentration of AIP as

$$a = \frac{kDB + \gamma R}{\lambda_a + \beta C} \overset{\lambda_a = 0}{\approx} \frac{kDB + \gamma R}{\beta C},$$

and obtain that $Ca \approx \frac{kDB + \gamma R}{\beta}$. Inserting this into the expression $R = \frac{\beta Ca}{\gamma + \lambda}$, we obtain that $R = \frac{kDB}{\lambda}$ and therefore with $B = M_2$ that

$$a = \frac{k(1 + \frac{\gamma}{\lambda})}{\beta}(1 + vP_{agr}).$$

Furthermore, for A_P we obtain that

$$A_P = \frac{\phi AR}{\mu + \lambda} = \frac{\phi \lambda M_2}{(\mu + \lambda)(\frac{\lambda^2}{kDB} + \phi) - \phi \mu} = \frac{1 + v P_{agr}}{(\mu + \lambda)\frac{\lambda + k(1 + v P_{agr})}{k\phi(1 + v P_{agr})^2} + 1}$$

and for the concentrations of PSM, amyloid fibrils and mRNAIII we calculate that

$$[PSM] = 1 + v_{PSM} P_{PSM}, \qquad f = D[PSM] = \frac{1 + v P_{agr}}{1 + \frac{k}{\lambda}(1 + v P_{agr})}(1 + v_{PSM} P_{PSM}),$$

$$R_3 = [\delta\text{-}toxin] = 1 + v_3 P_{agr}.$$

Using that $\frac{dX}{d\hat{\tau}} = \frac{dX}{dP_{act}}\frac{dP_{act}}{d\hat{\tau}}$, we obtain the following equations for the concentrations of AIP, PSM, δ-toxin and PIA:

$$\frac{da}{d\hat{\tau}} = \frac{k(1 + \frac{\gamma}{\lambda})}{\beta} v \frac{dP_{agr}}{d\hat{\tau}}, \qquad \frac{d[PSM]}{d\hat{\tau}} = v_{PSM} \frac{dP_{PSM}}{d\hat{\tau}},$$

$$\frac{d[\delta\text{-}toxin]}{d\hat{\tau}} = v_3 \frac{dP_{agr}}{d\hat{\tau}}, \qquad \frac{d[PIA]}{d\hat{\tau}} = v_{ica2}\frac{dP_{ica2}}{d\hat{\tau}}. \qquad (14)$$

Furthermore we use that $P_{agr} = \frac{1}{v}[\frac{\beta \lambda a}{k(\lambda + \gamma)} - 1]$ to obtain

$$A_P = \frac{a^3}{A_1 + A_2 a + A_3 a^2}, \qquad (15)$$

with the parameters $A_1 := \frac{k^2(\mu + \lambda)(\lambda + \gamma)^3}{\phi \beta^3 \lambda^2}$, $A_2 := \frac{k^2(\mu + \lambda)(\lambda + \gamma)^2}{\phi \beta^2 \lambda^2}$ and $A_3 := \frac{k(\lambda + \gamma)}{\beta \lambda}$.

The general solution of (11) is

$$P_{act}(\hat{\tau}) = \frac{\hat{b}_{act}[act+]}{\hat{b}_{act}[act+] + \hat{u}_{act}[act-]}$$

$$+ \left(P_{act,0} - \frac{\hat{b}_{act}[act+]}{\hat{b}_{act}[act+] + \hat{u}_{act}[act-]} \right) e^{-(\hat{b}_{act}[act+] + \hat{u}_{act}[act-])\hat{\tau}} \qquad (16)$$

and approaches the constant value exponentially fast. For the inter-cellular regulations to affect the proportions of up-regulated cells in another subsystem, a certain concentration of the substance has to be reached. These concentrations are thus taken as the steady state concentrations, which are obtained from (16) for $\hat{\tau} \to \infty$ as

$$\lim_{\hat{\tau} \to \infty} P_{act}(\hat{\tau}) = \frac{\hat{b}_{act}[act+]}{\hat{b}_{act}[act+] + \hat{u}_{act}[act-]}.$$

With A_P defined as in (15), the terms in (6) are determined by straight-forward calculations as

$$R_3 = 1 + \frac{v_3}{v}\left[\frac{\beta\lambda a}{k(\lambda + \gamma)} - 1\right], \tag{17}$$

$$[SarA] = 1 + v_{sarA}\frac{b_{sarA}(1 + v_\sigma f([str]))}{u_{sarA} + b_{sarA}(1 + v_\sigma f([str]))}, \tag{18}$$

$$[SarU] = 1 + v_{sarU}b_1\frac{K_1 + K_2a + (K_3 + K_4a)f([str])}{K_5 + K_2a + (K_6 + K_4a)f([str])}, \tag{19}$$

where

$$f([str]) := \frac{(b_0 + b_\sigma[str])[str]}{(b_0 + b_\sigma[str])[str] + u_\sigma}$$

and K_i, $i \in \{1, \ldots, 6\}$ as in Table 2. Thus $f([str])$ depends on the system stress in a limited growth process. By inserting the expressions from (15), (17)–(19) and $[\sigma^B] = 1 + v_\sigma f([str])$ into (14), the differential equation for the amount of free AIP is given as

$$\frac{da}{d\hat{\tau}} = C_{11}(C_1 - C_2a)\left[C_3 + C_4f([str]) + C_5a + C_6\frac{f([str])}{B_5 + f([str])}\right.$$
$$\left. +C_8\frac{K_1 + K_2a + (K_3 + K_4a)f([str])}{K_5 + K_2a + (K_6 + K_4a)f([str])} + \frac{a^3}{A_1 + A_2a + A_3a^2}\right]$$
$$-C_{11}(C_9 + C_{10}f([str])) \tag{20}$$

with the parameters C_i, $i \in \{1, \ldots, 11\}$ and B_5 as in Table 3.

PSM molecules enable the lysis of cells to gain nutrients. Due to abundant nutrient supply in the medium and a homogeneous bacteria population, cell lysis only plays a minor role and the concentration of PSM is not included explicitly. We remark however that an increase in the PSM concentration is positively influenced by the concentration of free AIP, i.e. *agr* activity. Furthermore, the equation for δ-toxin only differs by a

Table 2 Formulas for parameters K_i, $i \in \{1, \ldots, 6\}$

Parameter	Formula
K_1	$u_2\alpha v_{sarA}b_{sarA} + (b_1 + u_2(\alpha + 1 - \frac{v_3}{v}))(b_{sarA} + u_{sarA})$
K_2	$\frac{u_2\beta\lambda v_3}{vk(\lambda+\gamma)}(b_{sarA} + u_{sarA})$
K_3	$[u_2\alpha v_{sarA} + b_1 + u_2(\alpha + 1 - \frac{v_3}{v})]b_{sarA}v_\sigma$
K_4	$\frac{u_2\beta\lambda v_3}{vk(\lambda+\gamma)}b_{sarA}v_\sigma$
K_5	$(b_1 + u_1)K_1 + u_1v_{sarT}b_1(b_{sarA} + u_{sarA})$
K_6	$(b_1 + u_1)K_3 + u_1v_{sarT}b_1b_{sarA}v_\sigma$

Table 3 Formulas for parameters C_i, $i \in \{1, \ldots, 6, 8, \ldots, 11\}$ and B_5

Parameter	Formula	Parameter	Formula	Parameter	Formula
C_1	$b_{agr}(1 + \frac{1}{v})$	C_2	$b_{agr} \frac{\beta\lambda}{vk(\lambda+\gamma)}$	C_3	$1 + 2\alpha - \frac{v_3}{v} + \frac{u_{agr}}{b_{agr}}$
C_4	$\frac{u_{agr}}{b_{agr}} v_\sigma$	C_5	$\frac{v_3\beta\lambda}{vk(\lambda+\gamma)}$	C_6	αv_{sarA}
C_8	$\alpha v_{sarU} b_1$	C_9	u_{agr}	C_{10}	$u_{agr} v_\sigma$
C_{11}	$\frac{k(1+\frac{\gamma}{\eta})}{\beta} v$	B_5	$\frac{u_{sarA}}{b_{sarA} v_\sigma}$		

factor from that for free AIP. It inhibits spreading of the colony, which is used in the replicative bacteria diffusion term of the full model.

Inserting into (14) yields that the concentration of the main biofilm component PIA depends on the evolution of the proportion P_{ica2} as

$$\frac{d[PIA]}{d\hat{\tau}} = v_{ica2} \frac{dP_{ica2}}{d\hat{\tau}}$$
$$= v_{ica2}\left[b_{ica2}([SarA] + r_{ica2}n(1 - \frac{n}{K_n}))(1 - P_{ica2}) - u_{ica2}[IcaR]^2 P_{ica2}\right].$$

We insert the expression for $[SarA]$ from (18) and $P_{ica2} = \frac{[PIA]-1}{v_{ica2}}$ as well as $[IcaR] = 1 + v_{ica1} \frac{b_{ica1}}{b_{ica1}+u_{ica1}[str]}$. Using that $v_{ica2} \gg 1$, we simplify the equation to obtain

$$\frac{d[PIA]}{d\hat{\tau}} \approx \left[P_1 + P_2 \frac{f([str])}{B_5 + f([str])} + P_3 n(1 - \frac{n}{K_n})\right](P_4 - [PIA])$$
$$- \frac{P_5}{(P_6 + [str])^2}([PIA] - 1) \tag{21}$$

with the model parameters P_i, $i \in \{1, \ldots, 6\}$ described in Table 4.

Since the variable $[str]$ itself is a model assumption and $f([str]) \in [0, 1]$, the approximation $f([str]) \approx [str] \in [0, 1]$ allows a significant complexity reduction without loosing much information. Figure 7 shows the very good agreement between the full ODE model introduced in Sect. 2.1–2.4 and (20)–(21) with $f([str]) \approx [str]$. Parameter values are as indicated by magnitude considerations as in (13).

Table 4 Formulas for parameters P_i, $i \in \{1, \ldots, 6\}$

Parameter	Formula	Parameter	Formula	Parameter	Formula
P_1	b_{ica2}	P_2	$b_{ica2} v_{sarA}$	P_3	$b_{ica2} r_{ica2}$
P_4	v_{ica2}	P_5	$\frac{u_{ica2} b_{ica1}^2 v_{ica1}^2}{u_{ica1}^2}$	P_6	$\frac{b_{ica1}}{u_{ica1}}$

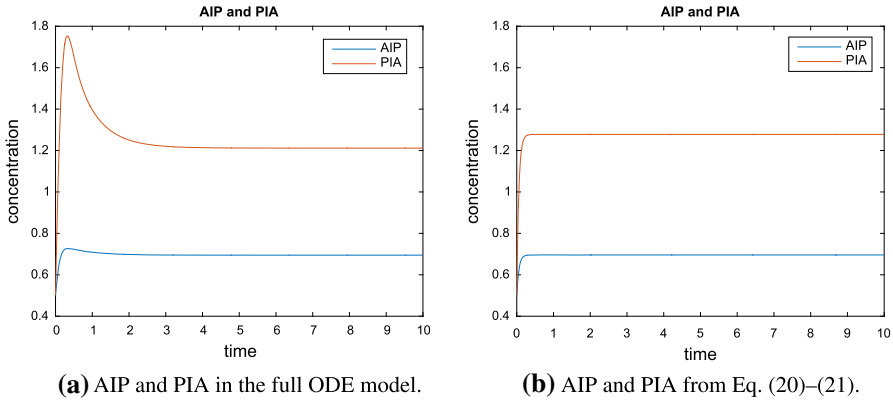**(a)** AIP and PIA in the full ODE model.   **(b)** AIP and PIA from Eq. (20)–(21).

Fig. 7 Concentrations of AIP and PIA from the full and the reduced ODE system (colour figure online)

2.6 Inclusion into the PDE model

In the following, we combine the derived ODE with adequate terms for the spread in space to obtain a PDE model for bacterial pattern formation. The concentration of the *S. aureus* QS substance AIP is denoted by q in the PDE model.

The evolution of the QS substance is obtained by multiplying the evolution of the AIP concentration with the density b of replicative bacteria, which can produce AIP. We derive $f_2(b, q)$ in (4) from (20) as

$$f_2(b, q) \approx G_q \, b \, (1 - \alpha q) \left[\beta_q \left(q + \alpha_3 \frac{q^3}{1 + c_1 q + c_2 q^2} \right) + \beta^\star_{str} \right.$$
$$\left. + \beta_{str,q} \frac{K_1 + K_2 q + (K_3 + K_4 q)[str]}{K_5 + K_2 q + (K_6 + K_4 q)[str]} \right] - \mu_{str} b. \tag{22}$$

Biofilm growth is determined by the principal biofilm component PIA, which is included explicitly with the concentration f. Although the production of PIA is not under the control of *agr* (Vuong et al. 2005), the *agr* system influences biofilm formation via other mechanisms since repression of *agr* is necessary to form biofilm and the reactivation of *agr* in established biofilms through AIP addition or glucose depletion triggers detachment (Boles and Horswill 2008). We include the *agr*-mediated biofilm detachment depending on the extracellular presence of AIP and $f_3(n, b, q, f)$ in (5) is obtained with (21) as

$$f_3(n, b, q, f) = b \, \frac{d[PIA]}{d\hat{\tau}} \frac{1}{1 + \beta_f q} - \mu_f \, f \, q$$
$$\approx G_f b \left[\left(\gamma^\star_{str} + \gamma_n n \left(1 - \frac{n}{K_n} \right) \right) (K_f - f) - \gamma^\star_{str,f} f \right] \frac{1}{1 + \beta_f q} - \mu_f \, f \, q. \tag{23}$$

Table 5 Formulas for additional parameters in the PDE model equations

Parameter	Formula	Parameter	Formula	Parameter	Formula
G_q	$C_1 C_3 C_{11}$	α	C_2/C_1	β_q	C_5/C_3
α_3	$1/(C_5 A_1)$	c_1	A_2/A_1	c_2	A_3/A_1
$\beta_{str}^\star$	$1 + \frac{C_4[str]}{C_3} + \frac{C_6[str]}{C_3(B_5+[str])}$	$\beta_{str,q}$	C_8/C_3	G_f	P_1
μ_{str}	$C_{11}(C_9 + C_{10}[str])$	$\gamma_{str}^\star$	$1 + \frac{P_2[str]}{P_1(B_5+[str])}$	γ_n	P_3/P_1
$\gamma_{str,f}^\star$	$\frac{P_5}{P_1(P_6+[str])^2}$	K_f	P_4	K_n, β_f, μ_f	Assumpt

Note that the parameters in (22) and (23) are as stated in Table 5. Furthermore the presence of the biofilm growth environment facilitates diffusion and especially nutrient transport in comparison to the situation where only bacteria are present, which is included into the nutrient diffusion term as

$$D_1(f) = d_n(1 + f). \tag{24}$$

Although *S. aureus* bacteria do not have a flagella, they are able to spread on soft agar with a velocity of approximately $100\frac{\mu m}{min}$. This spread is inhibited by the secretion of inhibitors against colony-spreading such as δ-toxin (Omae et al. 2012). Due to (14) and the fact that both concentrations are zero initially, we assume that $[\delta\text{-toxin}] = \alpha_q a$. Note that δ-toxin belongs to the family of PSM and inhibits colony spreading, but not the growth rate of *S. aureus* (Omae et al. 2012). Therefore it is included as a factor $\frac{1}{1+\alpha_q q}$ into the diffusion term of the bacteria and we obtain

$$D_2(n, b, q) = \frac{\sigma n b}{1 + \alpha_q q}. \tag{25}$$

Furthermore, we use Fickian diffusion for f as we consider the biofilm indicator molecule PIA. However, the involved modeling of the replicative bacteria diffusion also influences f as the presence of b is necessary for the production of PIA. We note that the choice of linear diffusion for the biofilm growth environment f allows this component to diffuse outside the colony, such that the bacteria can grow and spread in the growth environment.

Other PSM than δ-toxin, such as PSM-α and PSM-β, are stimulants of biofilm spreading (Omae et al. 2012), which are able to lyse eukaryotic cells, especially in competitive settings with several bacteria types (Cheung and Manna 2005). In PSM mutants, PSM-induced lysing is not available and thus the bacteria growth parameters G_1, G_2 in (1)–(2) are smaller than in the wildtype bacterium. Note that, since PSM production depends on the availability of phosphorylated AgrA, also *agr* mutants do not produce PSM and the same changes apply.

Amyloid fibrils provide structural integrity to biofilms (Romero et al. 2010) and increase resistance to degradation (Schwartz et al. 2012). The production of amyloid fibrils depends on the *agr* locus, such that in *agr* mutants, the diffusion coefficient σ

of the replicative bacteria increases. The substance α-toxin is necessary for cell-to-cell interaction during biofilm formation. Colonies of bacteria lacking α-toxin are unable to adhere to plastic surfaces under static or flow conditions (Caiazza and O'Toole 2003). Since the initial microbial adhesion to surfaces is a complex process involving bacterial factors as well as physical interactions like Lifshitz–van der Waals forces, electrostatic forces, acid-base interactions and Brownian motion forces (Cerca et al. 2005), we do not consider α-toxin effects. Protein A is most important in the context of invasion of a biological host (DeDent et al. 2007), where it facilitates colony spreading and virulence. In attachment or *spa* mutants the parameter δ in (1)–(2) is increased since a decrease in *spa* activity is linked to an increase in *agr* activity. Furthermore, the decrease in cell wall anchoring of protein A in the *spa* mutant decreases the stability of the biofilm, which results in an increased nutrient diffusion coefficient. The detailed mutant parameter changes are described in Table 7 in the following section.

3 Numerical simulation results and real data comparison

In this section we compare numerical simulations of our derived partial differential equations to biological observations of *S. aureus* pattern formation in the laboratory. The experimental observations are extracted from the published article by García-Betancur et al. (2017) and show *S. aureus* aggregates growing on top of an Mg^{2+}-enriched TSB medium (TSBMg), where clinical isolates can develop robust multicellular aggregates.

For the simulations of our system, we use a time-adaptive finite element method implemented in MATLAB. In this finite element method we use first order linear finite elements with mass lumping on a triangular unstructured grid (Braess 2003; Brenner and Scott 2008). These are then coupled to an implicit Euler method for the time discretization. Additionally, for the time discretization, the size of the time steps used here is steered by the amount of Newton steps needed to solve the linearized equation system. The time step size in our method takes values between an upper and a lower bound, which both ensure convergence of the method, and the adaptive choice of the time step speeds up the computations. Also a constant time step could be used for the computations. Furthermore, it should be noted that for all the following simulations convergence studies have been performed to avoid an influence of the grid on the resulting patterns.

We further use a random diffusion component from a triangular distribution and initial conditions as introduced by Kawasaki et al. (1997) to reflect the stochastic fluctuation of the random movement of bacteria and not fully homogeneous material properties. This means that the diffusion parameter σ has the form $\sigma = \sigma_0(1 + \Delta)$, where $\sigma_0 = 0.5$ and Δ is taken from a triangular distribution supported by $[-1, 1]$. This fluctuation is applied for every grid unit once in the initialization. Thus one parameter value is chosen randomly in order to break the symmetry of the solution. We note that simulation results without the random diffusion component show symmetric patterns as depicted in the paper by Horger et al. (2015).

As boundary conditions, we choose no-flux conditions as the colony grows on a nutrient medium dish which neither component can leave, i.e.

$$\frac{\partial n}{\partial \mathbf{x}}\Big|_{\partial \Omega} = \frac{\partial b}{\partial \mathbf{x}}\Big|_{\partial \Omega} = \frac{\partial s}{\partial \mathbf{x}}\Big|_{\partial \Omega} = \frac{\partial q}{\partial \mathbf{x}}\Big|_{\partial \Omega} = \frac{\partial f}{\partial \mathbf{x}}\Big|_{\partial \Omega} = 0,$$

where $\Omega \subset \mathbb{R}^2$ denotes the area of the dish, which corresponds to a rectangular computation domain. As the initial concentration of nutrients is homogeneous throughout the medium, we define the initial nutrient concentration as

$$n(\mathbf{x}, 0) = n_0$$

for $\mathbf{x} \in \Omega$ and $n_0 = 1.11$. Furthermore, the initial concentrations of non-replicative bacteria, quorum sensing and biofilm component are set to zero as these substances are not present initially. The replicative bacteria are inoculated as a drop in the center of the dish, which is reflected by the initial concentration

$$b(\mathbf{x}, 0) = b_M \exp\left(-\frac{x^2 + y^2}{6.25}\right),$$

where $b_M = 0.71$.

We note that in the region outside the colony we find the TSB medium, which is a liquid enrichment medium. It shows only very little resistance against spatial expansion, such that these effects can be neglected in our model, especially since the colony is growing on top of the medium. Nutrients are present in the entire computation domain Ω and diffusion takes place inside and outside the colony.

Furthermore, the experimentally observed colonies are three-dimensional structures, whose height is small compared to their radius. We thus consider a two-dimensional simulation domain, on which we add the densities of replicative (b) and non-replicative (s) bacteria as well as the concentration of PIA as a representative of biofilm environment density (f). In the experimental results, it is not possible to distinguish between the single components. Thus, for the comparison to the experimental observations, we consider $b + s + f$, as they together correspond to the visible and comparable part of the experimental microcolony. At this point it should also be noted that here the height of a structure can only be interpreted as a concentration level. Since the dimensionless concentration of PIA is in the range of 0–4.5, these values are indicated by a light blue color and the larger density values, which range up to 14 in areas where bacteria are present, are indicated by shades of yellow and red.

We observe that many colonies show a concentric ring structure. Outside this ring structure, fingering behavior takes place, which is mainly influenced by the replicative bacteria. The structure inside the ring is due to the accumulation of non-replicative bacteria and varies for different experiments, even for the same mutant. Thus the features of the experimental observations we focus on in the numerical simulations are the structure of the fingering pattern in the outer areas of the colonies, the presence of a ring, but not its explicit structure, and the prominence of the surrounding environment layer. In order to investigate the structure inside the ring further, the biological
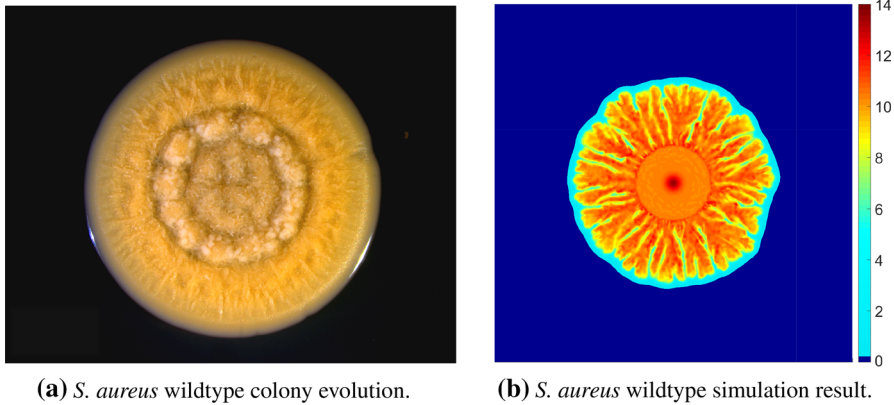
(a) *S. aureus* wildtype colony evolution.   **(b)** *S. aureus* wildtype simulation result.

Fig. 8 *S. aureus* wildtype simulation result obtained by adding b, s and f and using parameters in Table 6 in (**b**) in comparison to experimental observation by García-Betancur et al. (2017) in (**a**) (colour figure online)

Table 6 Non-dimensional parameter values for the simulation of the wildtype *S. aureus* bacteria colony

Parameter	Value	Parameter	Value	Parameter	Value	Parameter	Value
G_1	7	G_2	7	σ	0.5	G_f	0.1
G_q	0.1	μ_q	0.1	δ	1	d_n	1
d_f	2	d_q	1	ε	10	γ	1
q_m	0.3	z	1	τ	0.25	b_s	2
$1/a_1$	2400	$1/a_2$	120	ρ	1	α_q	1
α	0.1	β_q	1	α_3	100	c_1	1
c_2	100	$\beta_{str}^\star$	1	$\beta_{str,q}$	1	$K_1 = K_2$	1
K_3	10	K_4	10	K_5	1	K_6	10
$[str]$	0.5	$\gamma_{str}^\star$	1	γ_n	0.5	$\gamma_{str,f}^\star$	10
β_f	1	μ_f	0	K_f	10	K_n	10

Table 7 Changed parameter values for the simulation of the *S. aureus* mutant bacteria colonies in comparison to the wildtype parameters

Mutant	$G_1 = G_2$	σ	G_f	G_q	μ_q	δ	d_n	d_f
Wildtype	7	0.5	0.1	0.1	0.1	1	1	2
Ica	5	1	0	0.1	0.1	1	1	2
Spa	7	0.5	0.1	0.1	0.1	5	1.5	2
Ica and *spa*	5	1	0	0.1	0.1	5	1.5	2
Psm-α	6	0.5	0.1	0.1	0.1	1	0.7	2
Psm-β	4	0.65	0.1	0.1	0.1	1	0.4	3
Agr	2.5	0.6	0.1	0	0	1	0.5	2.5

processes underlying the transitions between the replicative and the non-replicative state as well as the interactions of the non-replicative bacteria with the environment could be studied in detail from a biological point of view and included into the dif-

ferential equations. The real data image for the wildtype bacterium in Fig. 8a shows a distinct structure with a concentric ring of bacteria and a narrow fingering or wrinkling structure towards the outer area of the colony. The colony is mostly round with only few very shallow dents. Furthermore, there is a layer surrounding the bacteria. For the wildtype bacterium we choose moderate parameter values as indicated in Table 6, since all regulation subsystems are active and contribute to the growth of the colony. The real data features are reproduced in the simulation result depicted in Fig. 8b, where a distinct ring structure is observed, the colony fingers are close and a layer of biofilm environment surrounds the colony.

The changes in the parameters for the mutant colonies are indicated in Table 7. In Fig. 9 the *ica*, *spa* and *ica/spa* mutant simulation results are depicted. In the real data in Fig. 9a, we observe that the extracellular matrix or *ica* mutant shows a less pronounced colony structure, especially in the inner area where the ring structure is weaker than in the wildtype colony. The colony is round, very narrow wrinkles are observed in the outer parts and the colony is not surrounded by a layer. The parameters $G_f = \mu_f = 0$ are chosen since the *ica* locus is deactivated. Furthermore the lack of biofilm environment leads to a slower availability of nutrients for colony growth, such that the growth rates G_1 and G_2 are decreased, and without the added structure of the biofilm, the bacteria move faster. In the simulation results depicted in Fig. 9b we observe that a good agreement is reached as the ring structure is less pronounced and the branches are very close.

In the attachment mutant, depicted in Fig. 9c, the *spa* locus is disabled. A very pronounced ring structure is observed and, in comparison to the wildtype, the spaces between the wrinkles in the outer part of the colony are larger. The colony is surrounded by a layer. Since a decrease in the concentration of protein A is linked to an increase in the AIP concentration, we increase the parameter δ. Protein A binds to the cell wall envelope (DeDent et al. 2007), thus providing stability to the biofilm. Due to the decreased stability, we slightly increase the nutrient diffusion coefficient d_n. In the simulation result in Fig. 9d we observe a good agreement of the simulations as the distances between the fingers are increased, while a very distinct ring structure is observed.

The combined *spa* and *ica* mutant in Fig. 9e shows features from both mutations. Here the concentric ring structure is more pronounced than in the *ica* mutant and the outer areas of the colony show wider gaps between the wrinkles in the colony structure. As above, there is no biofilm formation due to the *ica* locus mutation. In the simulation we combine the parameters G_1, G_2 and σ from the *ica* mutant with the parameters δ and d_n from the *spa* mutant to obtain the simulation result depicted in Fig. 9f. In comparison to Fig. 9b, it shows a stronger ring structure and wider gaps between the fingers, and thus a good agreement of the real data and the simulation.

Figure 10 shows the simulation results for the *psm-α* and *psm-β* mutants. The amyloid type 1 or *psm-α* mutant real data in Fig. 10a shows a pronounced ring structure and very narrow wrinkling in the outer areas of the round colony. In comparison to the wildtype colony, we observe a more prominent layer of biofilm environment surrounding the colony. Due to the lack of PSM, the POPC vesicle lysing capacity decreases. Since this capacity is smaller for PSM-α than for PSM-β, also the decrease is smaller. Due to the structuring effect of PSM, we decrease the parameter d_n. Since

(a) *Ica* mutant colony evolution.

(b) *Ica* mutant simulation result.

(c) *Spa* mutant colony evolution.

(d) *Spa* mutant simulation result.

(e) *Ica* and *spa* mutant colony evolution.

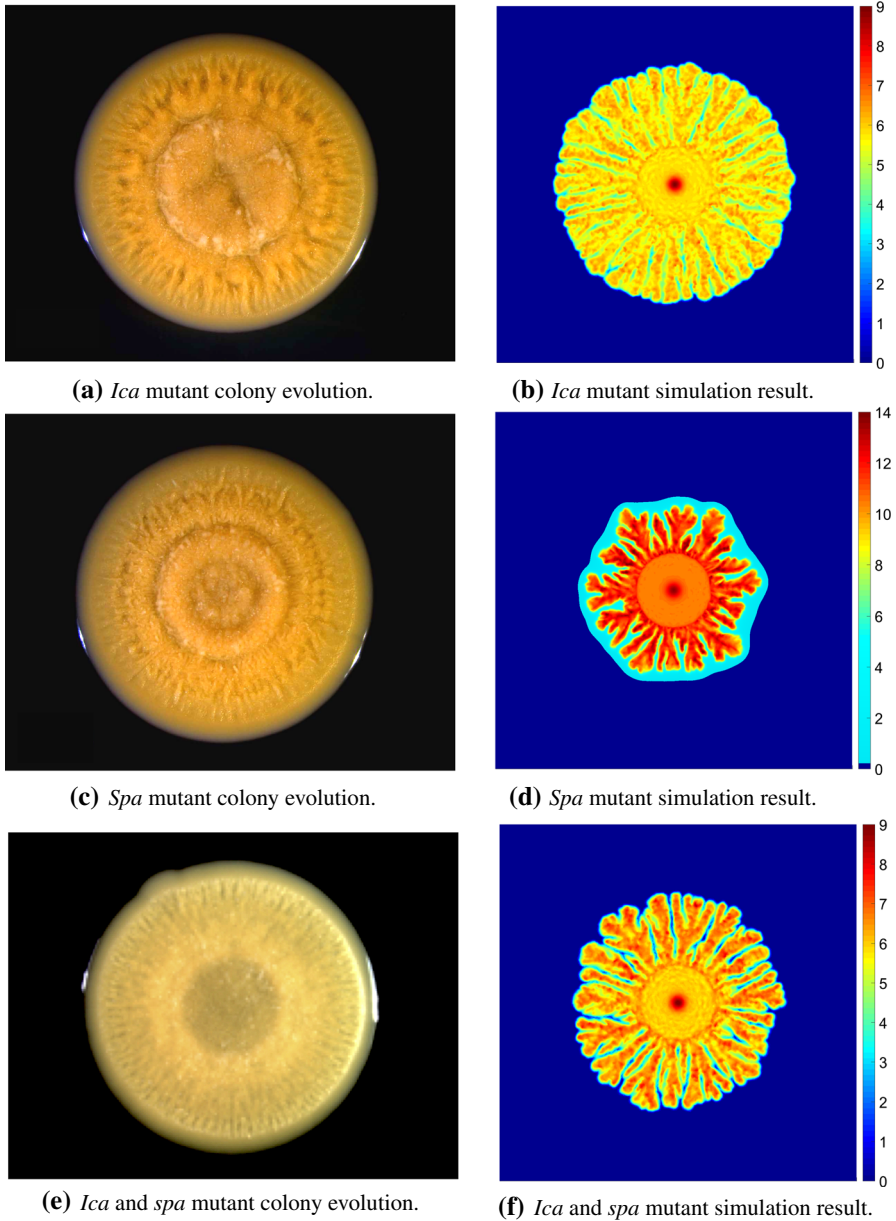**(f)** *Ica* and *spa* mutant simulation result.

Fig. 9 *Ica* and *spa* mutant simulations obtained by adding b, s and f on the right and experimental observations by García-Betancur et al. (2017) on the left (colour figure online)

the *psm-α* mutation has slighter effects than the *psm-β* mutation on biofilm diffusion, we do not change the parameter d_f here. The described changes in colony morphology are reproduced in the simulation result depicted in Fig. 10b. For the amyloid type 2 or

(a) *Psm-α* mutant colony evolution.

(b) *Psm-α* mutant simulation result.

(c) *Psm-β* mutant colony evolution.

(d) *Psm-β* mutant simulation result.
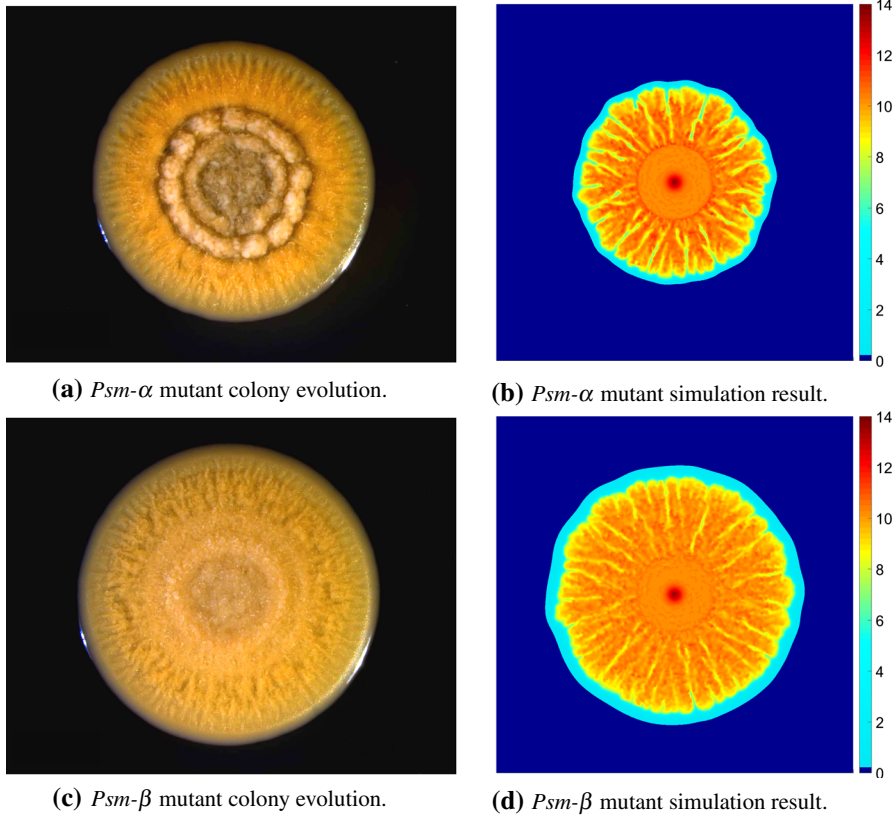
Fig. 10 *S. aureus psm-α* and *psm-β* mutant simulation results obtained by adding b, s and f with described parameter changes on the right and experimental observations by García-Betancur et al. (2017) on the left (colour figure online)

psm-β mutant depicted in Fig. 10c, we also slightly increase the replicative bacteria diffusion parameter since the lack of biofilm structure facilitates bacteria movement. We again decrease d_n and, in contrast to the *psm-α* mutant, we increase d_f to obtain the simulation results depicted in Fig. 10d, where again a good agreement of the simulation result is observed as very little structure and very little wrinkling are observed in a round colony shape.

The QS or *agr* mutant real data displayed in Fig. 11a shows a distinct structure in the middle of the colony, while towards the outer areas, the colony flattens and shows more pronounced dents. The colony is surrounded by a slightly uneven layer. Since the *agr* locus is not active, we take $G_q = \mu_q = 0$. No *agr* activity also means that there are no PSM, and thus the growth parameters are decreased as in the *psm* mutant colony. Furthermore, since the biofilm is less structured without PSM, the diffusion coefficient of the replicative bacteria is increased and the diffusion parameters for nutrients and biofilm are chosen between the values for the *psm-α* and *psm-β* mutant colonies. This is due to the fact that biofilm-enhancing effects in *psm-α* and *psm-β* mutants do not seem to be additive, as in *S. epidermidis* (Le et al. 2014; Wang et al.
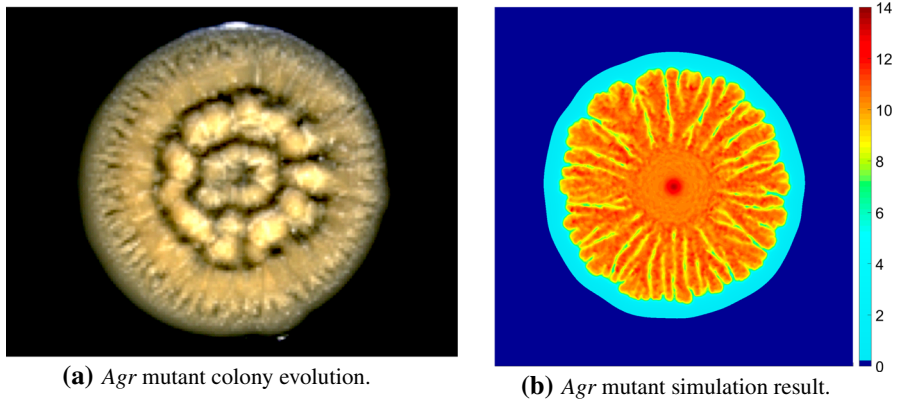
(a) *Agr* mutant colony evolution.

(b) *Agr* mutant simulation result.

Fig. 11 *S. aureus agr* mutant simulation result obtained by adding b, s and f with described parameter changes in (**b**) and experimental observation by García-Betancur et al. (2017) in (**a**) (colour figure online)

2011). We observe a good agreement of the simulation result depicted in Fig. 11b, where the structure in the middle of the colony as well as the slightly uneven layer are reproduced.

4 Conclusion

We investigated pattern formation in several mutant colonies of the bacterium *S. aureus*. Starting from the mathematical modeling of the *agr*, *sarA*, *ica* and *sarA* homologue cellular gene regulation systems, we derived a system of non-dimensional ordinary differential equations. Time-scale arguments and parameter size considerations allowed us to significantly reduce the system complexity, yielding differential equations and diffusion functions for the effects of quorum sensing and biofilm, where the parameters for the mutant colonies were derived from the gene regulations. We developed a new model for pattern formation in *S. aureus* and, in order to compare our results to experimental observations, we performed finite element simulations for several mutant colonies. Using the parameter changes indicated by the gene regulation mechanisms, we were able to adequately display the qualitative biological features of pattern formation in the simulations, thus establishing a basis for qualitative predictions of *S. aureus* pattern formation, which improves existing models by a reliable prediction of mutant colony growth. This work therefore constitutes a foundation for the further study of complex mutations in multiple gene loci.

References

Arciola CR, Campoccia D, Ravaioli S, Montanaro L (2015) Polysaccharide intercellular adhesin in biofilm: structural and regulatory aspects. Front Cell Infect Microbiol 5:7

Audretsch C, Lopez D, Srivastava M, Wolz C, Dandekar T (2013) A semi-quantitative model of quorum-sensing in *Staphylococcus aureus*, approved by microarray meta-analyses and tested by mutation studies. Mol BioSyst 9(11):2665–2680

Ballal A, Manna AC (2009) Expression of the sarA family of genes in different strains of *Staphylococcus aureus*. Microbiology 155:2342–2352

Ben-Jacob E, Cohen I, Golding I, Kozlovsky Y (2001) Modelling branching and chiral colonial patterning of lubricating bacteria. In: Maini PK, Othmer HG (eds) Mathematical models for biological pattern formation. Springer, Berlin, pp 211–253

Bischoff M, Entenza JM, Giachino P (2001) Influence of a functional sigB operon on the global regulators sar and agr in *Staphylococcus aureus*. J Bacteriol 183(17):5171–5179

Boles BR, Horswill AR (2008) Agr-mediated dispersal of *Staphylococcus aureus* biofilms. PLoS Pathog 4(4):e1000052

Braess D (2003) Finite Elemente: Theorie, schnelle Löser und Anwendungen in der Elastizitätstheorie, 3rd edn. Springer, Berlin

Brenner S, Scott R (2008) The mathematical theory of finite element methods, 3rd edn. Springer, Berlin

Bronner S, Monteil H, Prevost G (2004) Regulation of virulence determinants in *Staphylococcus aureus*: complexity and applications. FEMS Microbiol Rev 28:183–200

Caiazza NC, O'Toole GA (2003) Alpha-toxin is required for biofilm formation by *Staphylococcus aureus*. J Bacteriol 185(10):3214–3217

Cerca N, Brooks JL, Jefferson KK (2008) Regulation of the intercellular adhesin locus regulator (icaR) by sarA, sigmaB, and icaR in *Staphylococcus aureus*. J Bacteriol 190(19):6530–6533

Cerca N, Pier GB, Vilanova M, Oliveira R, Azeredoa J (2005) Quantitative analysis of adhesion and biofilm formation on hydrophilic and hydrophobic surfaces of clinical isolates of *Staphylococcus epidermidis*. Res Microbiol 156(4):506–514

Cheung AL, Manna AC (2005) Role of the distal sarA promoters in SarA expression in *Staphylococcus aureus*. Infect Immun 73(7):4391–4394

Cue D, Lei MG, Lee CY (2012) Genetic regulation of the intercellular adhesion locus in staphylococci. Front Cell Infect Microbiol 2:38

DeDent AC, McAdow M, Schneewind O (2007) Distribution of protein A on the surface of *Staphylococcus aureus*. J Bacteriol 189(12):4473–4484

Dervaux J, Carmelo Magniez J, Libchaber A (2014) On growth and form of Bacillus subtilis biofilms. Interface Focus 4(6):20130051

Dunman PM, Murphy E, Haney S, Palacios D, Tucker-Kellogg G, Wu S, Brown EL, Zagursky RJ, Shlaes D, Projan SJ (2001) Transcription profiling-based identification of *Staphylococcus aureus* genes regulated by the agr and/or sarA loci. J Bacteriol 183(24):7341–7353

Duong AC, Cheung GYC, Otto M (2012) Interaction of phenol-soluble modulins with phosphatidylcholine vesicles. Pathogens 1:3–11

Fuqua WC, Winans SC, Greenberg EP (1994) Quorum sensing in bacteria: the LuxR-LuxI family of cell density-responsive transcriptional regulators. J Bacteriol 176(2):269–275

García-Betancur JC, Goñi-Moreno A, Horger T, Schott M, Sharan M, Eikmeier J, Wohlmuth B, Zernecke A, Ohlsen K, Kuttler C, Lopez D (2017) Cell differentiation defines acute and chronic infection cell types in *Staphylococcus aureus*. eLife 6:e28023

Gray B, Hall P, Gresham H (2013) Targeting agr- and agr-like quorum sensing systems for development of common therapeutics to treat multiple Grampositive bacterial infections. Sensors 13(4):5130–5166

Horger T, Kuttler C, Wohlmuth B, Zhigun A (2015) Analysis of a bacterial model with nutrient-dependent degenerate diffusion. Math Methods Appl Sci 38(17):3851–3865

Jabbari S, King JR, Williams P (2012a) Cross-strain quorum sensing inhibition by *Staphylococcus aureus*. Part 1: a spatially homogeneous model. Bull Math Biol 74(6):1292–1325

Jabbari S, King JR, Williams P (2012b) Cross-strain quorum sensing inhibition by *Staphylococcus aureus*. Part 2: a spatially inhomogeneous model. Bull Math Biol 74(6):1326–1353

Jabbari S, King JR, Koerber AJ, Williams P (2010) Mathematical modelling of the agr operon in *Staphylococcus aureus*. J Math Biol 61:17–54

Kawasaki K, Mochizuki A, Matsushita M, Umeda T, Shigesada N (1997) Modeling spatio-temporal patterns generated by *Bacillus subtilis*. J Theor Biol 188(2):177–185

Knobloch JK-M, Jäger S, Horstkotte MA, Rohde H, Mack D (2004) RsbU-dependent regulation of Staphylococcus epidermidis biofilm formation is mediated via the alternative sigma factor sigmaB by repression of the negative regulator gene icaR. Infect Immun 72(7):3838–3848

Le KY, Dastgheyb S, Ho TV, Otto M (2014) Molecular determinants of staphylococcal biofilm dispersal and structuring. Front Cell Infect Microbiol 4:167

Manna AC, Cheung AL (2003) SarU, a sarA homolog, is repressed by SarT and regulates virulence genes in *Staphylococcus aureus*. Infect Immun 71(1):343–353

Matsushita M, Wakita J, Itoh H, Watanabe K, Arai T, Matsuyama T, Sakaguchi H, Mimura M (1999) Formation of colony patterns by a bacterial cell population. Physica A 274:190–199

Mhatre E, Gallegos Monterrosa R, Kovács ÁT (2014) From environmental signals to regulators: modulation of biofilm development in Gram-positive bacteria. J Basic Microbiol 54:1–17

Mimura M, Sakaguchi H, Matsushita M (2000) Reaction–diffusion modelling of bacterial colony patterns. Physica A 282:283–303

Müller J, Kuttler C, Hense BA, Rothballer M, Hartmann A (2006) Cell-cell communication by quorum sensing and dimensionreduction. J Math Biol 53:672–702

Omae Y, Sekimizu K, Kaito C (2012) Inhibition of colony-spreading activity of *Staphylococcus aureus* by secretion of delta-hemolysin. J Biol Chem 287:15570–15579

Pane-Farre J, Jonas B, Hardwick SW, Gronau K, Lewis RJ, Hecker M, Engelmann S (2009) Role of RsbU in controlling sigB activity in *Staphylococcus aureus* following alkaline stress. J Bacteriol 191(8):2561–2573

Perez-Velazquez J, Gölgeli M, Garcia-Contreras R (2016) Mathematical modelling of bacterial quorum sensing: a review. Bull Math Biol 78:1585–1639

Periasamy S, Joo H-S, Duong AC, Bach T-HL, Tan VY, Chatterjee SS, Cheung GYC, Otto M (2012) How *Staphylococcus aureus* biofilms develop their characteristic structure. PNAS 109(4):1281–1286

Peschel A, Otto M (2013) Phenol-soluble modulins and staphylococcal infection. Nat Rev Microbiol 11:667–673

Queck SY, Jameson-Lee M, Villaruz AE, Bach T-HL, Khan BA, Sturdevant DE, Ricklefs SM, Li M, Otto M (2008) RNAIII-independent target gene control by the agr quorumsensing system: insight into the evolution of virulence regulation in *Staphylococcus aureus*. Mol Cell 32(1):150–158

Romero D, Aguilar C, Losick R, Kolter R (2010) Amyloid fibers provide structural integrity to *Bacillus subtilis* biofilms. PNAS 107(5):2230–2234

Schmidt KA, Manna AC, Cheung AL (2003) SarT influences sarS expression in *Staphylococcus aureus*. Infect Immun 71(9):5139–5184

Schwartz K, Sekedat MD, Syed AK, O'Hara B, Payne DE, Lamb A, Boles BR (2012) Functional amyloids composed of phenol soluble modulins stabilize *Staphylococcus aureus* biofilms. PLoS Pathog 8(6):e1002744

Schwartz K, Sekedat MD, Syed AK, O'Hara B, Payne DE, Lamb A, Boles BR (2014) The AgrD N-terminal leader peptide of *Staphylococcus aureus* has cytolytic and amyloidogenic properties. Infect Immun 82(9):3837–3844

Seminara A, Angelini TE, Wilking JN, Vlamakis H, Ebrahim S, Kolter R, Weitz DA, Brenner MP (2012) Osmotic spreading of Bacillus subtilis biofilms driven by an extracellular matrix. PNAS 109(4):1116–1121

Senn MM, Giachino P, Homerova D, Steinhuber A, Strassner J, Kormanec J, Flückiger U, Berger-Bächi B, Bischoff M (2005) Molecular analysis and organization of the sigmaB operon in *Staphylococcus aureus*. J Bacteriol 187(23):8006–8019

Valle J, Toledo-Arana A, Berasain C, Ghigo JM, Amorena B, Penades JR, Lasa I (2003) SarA and not sigmaB is essential for biofilm development by *Staphylococcus aureus*. Mol Microbiol 48(4):1075–1087

Vlamakis H, Chai Y, Beauregard P, Losick R, Kolter R (2013) Sticking together: building a biofilm the *Bacillus subtilis* way. Nat Rev Microbiol 11(3):157–168

Vuong C, Kidder JB, Jacobson ER, Otto M, Proctor RA, Somerville GA (2005) *Staphylococcus epidermidis* polysaccharide intercellular adhesin production significantly increases during tricarboxylic acid cycle stress. J Bacteriol 187(9):2967–2973

Wang R, Khan BA, Cheung GYC, Bach T-HL, Jameson-Lee M, Kong K-F, Queck SY, Otto M (2011) *Staphylococcus epidermidis* surfactant peptides promote biofilm maturation and dissemination of biofilm-associated infection in mice. J Clin Investig 121(1):238–248

Ward JP, King JR, Koerber AJ, Williams P, Croft JM, Sockett RE (2001) Mathematical modelling of quorum sensing in bacteria. IMA J Math Appl Med Biol 18:263–292

Waters LS, Storz G (2009) Regulatory RNAs in bacteria. Cell 136(4):615–628

Xu L, Li H-, Vuong C, Vadyvaloo V, Wang J, Yao Y, Otto M, Gao Q (2006) Role of the luxS quorum-sensing system in biofilm formation and virulence of *Staphylococcus epidermidis*. Infect Immun 74(1):488–496

Yarwood JM, Schlievert PM (2003) Quorum sensing in Staphylococcus infections. J Clin Invest 112(11):1620–1625

Yarwood JM, Bartels DJ, Volper EM, Greenberg EP (2004) Quorum sensing in *Staphylococcus aureus* biofilms. J Bacteriol 186(6):1838–1850

Zhao L, Xue T, Shang F, Sun H, Sun B (2010) *Staphylococcus aureus* AI-2 quorum sensing associates with the KdpDE two-component system to regulate capsular polysaccharide synthesis and virulence. Infect Immun 78:3506–3515